Weisfeiler-Lehman Graph Kernel Method:
A New Approach to Weak Chemical Tagging

Yuan-Sen Ting [* 1 2 3]   **Bhavesh Sharma** [* 2]

Abstract

Stars' chemical signatures provide invaluable insights into stellar cluster formation. This study utilized the Weisfeiler-Lehman (WL) Graph Kernel to examine a 15-dimensional elemental abundance space. Through simulating chemical distributions using normalizing flows, the effectiveness of our algorithm was affirmed. The results highlight the capability of the WL algorithm, coupled with Gaussian Process Regression, to identify patterns within elemental abundance point clouds correlated with various cluster mass functions. Notably, the WL algorithm exhibits superior interpretability, efficacy and robustness compared to deep sets and graph convolutional neural networks and enables optimal training with significantly fewer simulations ($\mathcal{O}(10)$), a reduction of at least two orders of magnitude relative to graph neural networks.

1. Introduction

Over the past decade, innovative spectroscopic surveys, such as Gaia-ESO, APOGEE, GALAH, and LAMOST, have significantly advanced our understanding of the Milky Way (Gilmore et al., 2012; Luo et al., 2015; Majewski et al., 2017; Buder et al., 2020). These surveys have generated detailed mappings of the galaxy, capturing complex chemical profiles of $10^5 - 10^7$ stars. Consequently, we have extensive data on up to 30 different elements within each star, surpassing the scope of past research that was limited to a few thousand high-quality stellar spectra (Fuhrmann, 1998; Bensby et al., 2003).

---
[*]Equal contribution [1]Research School of Astronomy & Astrophysics, Australian National University, Cotter Rd., Weston, ACT 2611, Australia [2]School of Computing, Australian National University, Acton, ACT 2601, Australia [3]Department of Astronomy, The Ohio State University, Columbus, USA. Correspondence to: Yuan-Sen Ting <yuan-sen.ting@anu.edu.au>, Bhavesh Sharma <Bhavesh.Sharma@anu.edu.au>.

However, conventional analysis methods for this rich, high-dimensional dataset often lean on outdated models developed before the advent of comprehensive spectroscopic surveys. Many of these models oversimplify the multidimensional chemical space by focusing on chemical tracks and neglect its broader complexity (Weinberg et al., 2019; Griffith et al., 2019; 2020; Buck et al., 2021; Chen et al., 2022). Furthermore, these models typically presume that stars are independently drawn from a parent distribution, failing to consider the formation of stars in clusters or aggregates.

Stars originate within clusters, spreading throughout the galaxy and leaving distinct chemical signatures (Li et al., 2019; Just et al., 2023). These tags offer precious insights into star cluster formation and dispersal (Freeman & Bland-Hawthorn, 2002; Spina et al., 2022). Studying these tags affords us an understanding of the early stages of the Milky Way's evolution and its dynamic states, as the formation conditions and aggregations of stars mirror the galaxy's turbulence state (Ha et al., 2021; Smith et al., 2022).

Despite its potential, chemical tagging—the identification of unique clusters via the multidimensional space of elemental abundances—has shown limitations. While different cluster mass functions generate unique patterns within the elemental abundance space, the paucity of chemical volume currently hampers our capacity to identify individual clusters directly (Ting et al., 2015; Ness et al., 2018; Price-Jones & Bovy, 2018). Instead, the underlying cluster mass function is inferred through robust summary statistics that capture subtle variations in point cloud morphology.

This study introduces a novel approach to the complexities of statistical chemical tagging, employing a graph-based kernel method. Our methodology is inspired by the well-explored field of graph isomorphism and its ties with graph kernels, a domain extensively investigated in machine learning (Kriege et al., 2020). To our knowledge, this potent technique has not been previously utilized in astronomy. Our aim is to demonstrate the potential of the Weisfeiler-Lehman graph kernel method (Shervashidze et al., 2011; Morris et al., 2017; Schulz et al., 2022), known for its simple yet powerful formalism, in advancing the statistical study of stellar population chemical properties.
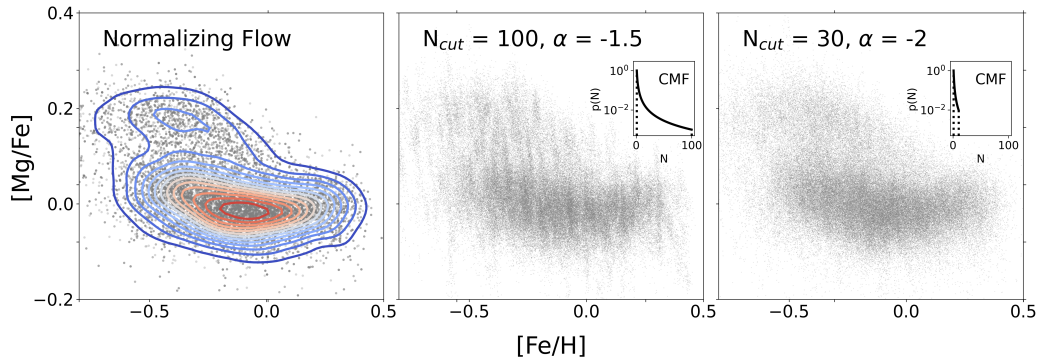
Figure 1. Weak chemical tagging. The plot presents a 2D projection of a complex 15D elemental abundance space. The left panel displays the smooth distribution, determined from the APOGEE data via a normalizing flow. The central and right panels depict varying Milky Way stochastic chemical evolution scenarios. Incorporating larger star clusters through an elevated mass cutoff, N_{cut}, or a subdued power-law gradient, α, leads to increased clustering in the chemical space.

2. Data and Simulations

Our model is based on a high-quality subset from the APOGEE DR16 survey (Weinberg et al., 2019), including stars from the Milky Way disk situated within a 3-13 kpc radius from the Galactic center and within 2 kpc of the Galactic plane. We focus on stars with a surface gravity between 1 and 2.5 and effective temperatures from 4100 K to 4600 K. These stars provide precise estimates of the abundance of 15 elements from APOGEE: Mg, O, Si, S, Ca, Na, Al, K, V, Cr, Mn, Fe, Co, Ni, and Cu (Jönsson et al., 2020; Vincenzo et al., 2021).

We utilize a normalizing flow model, trained on this dataset, to emulate the distribution within a 15-dimensional elemental abundance space. The model translates the complex distribution into a unit-multivariate Gaussian distribution through invertible neural networks. This allows us to sample from the distribution by first sampling from the unit Gaussian, then performing the inverse transformation. Our normalization flow includes eight units of Neural Spline Flow and GLOW (Kingma & Dhariwal, 2018; Durkan et al., 2019), each containing three densely connected layers with 16 neurons.

We populate chemically analogous star clusters within this 15D space. We posit that the number of observed stars follows a power-law distribution $N \sim N^{-\alpha}$, characterized by the power law slope α and a high-mass cutoff of N_{cut} (Dessauges-Zavadsky & Adamo, 2018; Mok et al., 2019). The elemental abundances of all stars within a cluster are derived from $\mathbb{R}^{15} \ni \mathbf{x} \sim \mathcal{N}(\mathbf{x_c}, \Sigma)$, with Σ representing the abundance dispersion due to measurement uncertainties. The centroid $\mathbf{x_c}$ is drawn from the smooth distribution estimated by the normalizing flow, and the measurement dispersion Σ from the determinations from Jönsson et al. (2020). Varying physical conditions of gas fragmentation, represented in the power law slope and high-mass cutoff, can result in subtle yet significant clustering properties of

the point clouds, as demonstrated in Fig. 1.

We note that, for the high-mass cutoff N_{cut}, it doesn't insinuate clusters initially contained such a limited number of stars. Our current million-star sample captures a minuscule fraction due to the Milky Way's vast parent sample. Notably, the current survey of 10^6 stars generally results in a subsampling fraction of 10^{-5} from the parent distribution of the entire Milky Way (Ting et al., 2015; 2016). Consequently, $N_{\text{cut}} = 10$ corresponds to a star cluster of $M \simeq 10^6 M_\odot$.

3. Methods

Weisfeiler-Lehman Graph Kernel: In the era preceding the emergence of graph neural networks (GNNs) as tools for graph representation, kernel methods were the primary choice for tasks involving graph prediction. However, one of the most prominent challenges that arose during the application of these kernel methods to graphs was formulating an efficient similarity measure.

To address this problem, the Weisfeiler-Lehman (WL) kernel method was developed to generate features that capture the inherent structure of input graphs. For a graph $G = (V, E)$, with V representing nodes and $E \subseteq V \times V$ denoting edges, the neighbourhood of a node v is defined as $\mathcal{N}(v) = \{u \mid (u, v) \in E\}$. In our situation, we start with point clouds in the elemental abundance space that lack edges. We then impose a graph structure by connecting nodes that are within a Euclidean distance of less than 0.15 dex in a 15-dimensional space. The radius for this is obtained through a hyperparameter grid search, and the degree of individual nodes serves as the initial node attributes.

The WL algorithm is designed to refine node attributes iteratively by incorporating local information. For a given node v, a multiset of neighbouring attributes is established and then distilled into a unique embedding l_i via an injective function f. The WL kernel method determines the graph
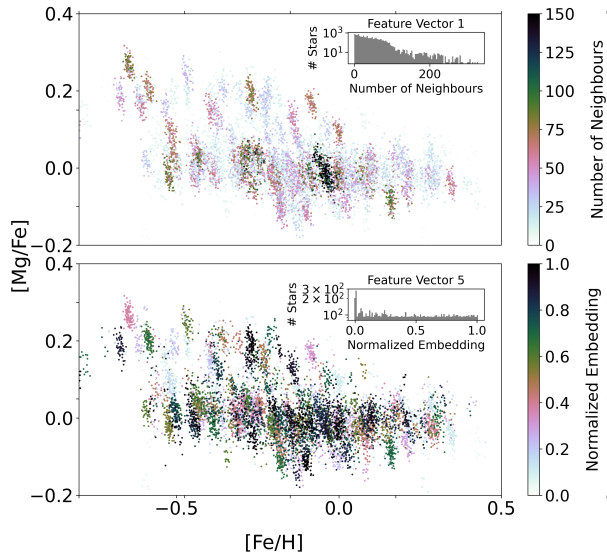
Figure 2. Initiating with the neighbour count within a predetermined radius (Top Panel), the WL kernel creates an aggregate embedding tuple for hierarchical similarity analysis. Post five iterations, nodes are colour-coded per WL embedding (Bottom Panel). The similarity between graphs is gauged via the dot product of the histogram of these successive embeddings, functioning as feature vectors (shown in the Inset Panels).

similarity by conducting a set number of iterations to create a feature map of the graph, $\phi(G)$, which is the histogram vector of the node embedding l_i. The pseudocodes are listed in Table 1 (refer to Fig.2). The similarity of two graphs, or the kernel $k(G, G')$, is then defined as the inner product of their respective features: $k(G, G') = \phi(G)^T \phi(G')$. The optimal number of iterations, found to be five in our case, through hyperparameter grid search.

We perform inference on the target label $\mathbf{y} = (\boldsymbol{\alpha}, \boldsymbol{N_{cut}})$ using a zero-mean Gaussian Process (GP) and the graph kernel as a similarity measure for observed graphs. For any new graph G_*, its target value y_* is predicted by a weighted sum of known $\mathbf{y}$ values, with weights derived from the WL kernel-based similarity between G_* and the training graphs $\mathbf{G}$. The mean prediction of y_* from GP is computed as $y_* = k(G_*, \mathbf{G})k(\mathbf{G}, \mathbf{G})^{-1}\boldsymbol{y}$, indicating that the new graph's target value prediction depends on its similarity to training graphs and the training labels

To holistically evaluate our method, we juxtapose it with two techniques: Deep Sets and Graph Neural Networks.

Deep Set Method: In this model, feature vectors $\tau(u) \in \mathbb{R}^{k+n}$ are constructed for each node u in a given graph realization G. This includes quantifying neighbours within a series of k radii, $r_k \in \{0.01, 0.05, 0.10, 0.15, 0.20\}$, and using n-dimensional positional information to distinguish isolated and densely populated clusters. The model output on an elemental abundance graph G is then given by, $\phi\left(\bigoplus_{u \in G} \psi(\tau(u))\right)$. Here, ψ transforms the feature vectors

---

Algorithm 1 The Weisfeiler-Lehman Algorithm

Input: Graphs $G_1, \ldots, G_N$, Total number of WL iterations h, Injective function f
for $i = 1$ **to** N **do**
$\quad l_i(v) \leftarrow |\mathcal{N}(v)|, \forall v \in G_i$
$\quad$ **for** $k = 1$ **to** h **do**
$\quad\quad l'_i(v) \leftarrow f(l_i(v), \{\!\{l_i(u) \mid u \in \mathcal{N}(v)\}\!\}), \forall v \in G_i$
$\quad\quad l_i \leftarrow l'_i$
$\quad$ **end for**
end for
Return Histogram of graph embeddings $l_i : V_i \to \mathbb{N}$, from all iterations as features for $G_1, \ldots, G_N$.

---

and is given by a learnable multi-layer perceptron (MLP) with a single layer, $\bigoplus$ is a mean aggregation operation, and ϕ is another single-layer MLP that maps the aggregated vector representation to parameters $y = (\alpha, N_{cut})$.

Convolutional Graph Neural Network (ConvGNN): The ConvGNN model addresses non-uniform data distributions by preserving isolated clusters' statistics through local aggregation. Each node $u \in G$ has a hidden representation $\mathbf{h}_u$, updated through a single GNN message-passing layer, and defined by $\mathbf{h}_u = \phi\left(\tau(u), \bigoplus_{v \in \mathcal{N}(u)} \psi(\tau(v))\right)$, where ψ and ϕ are learnable MLPs and $\bigoplus$ is a mean aggregation function. The node-level representations are averaged with a readout function $\mathcal{R}$ and passed through another single-layer MLP ρ, $\rho\left(\mathcal{R}(\{\mathbf{h}_u \mid u \in G\})\right)$ to infer the physical parameter $y = (\alpha, N_{cut})$, effectively leveraging the structural information of the graphs.

4. Results

This study demonstrates the potent potential of the WL algorithm in mining intrinsic physical parameters from elemental abundance point clouds. Through $5,000$ distinct chemical abundance simulations—each characterized by a unique power-law slope α and high-mass cutoff N_{cut}—we evaluate the performance and versatility of the WL algorithm.

Efficacy and Robustness: We measure efficacy by the minimum training samples necessary to ensure reliable results, quantified via the R² score and RMSE of the power-law slope recovery α (refer to Fig 3). Considering the extensive training times of ConvGNN, we narrow our scenario by setting N_{cut} at 100 and taking $\alpha \sim \mathcal{U}(-2.5, -1.5)$.

The WL algorithm's edge over deep-set and ConvGNN methods is unmistakable from Fig 3, excelling in interpreting nuanced elemental abundance data. Even with minimal simulations—on the order of $\mathcal{O}(1) - \mathcal{O}(10)$—the WL kernel accurately infers the underlying parameters, outperforming alternatives that rely on significantly larger datasets—on the order of $\mathcal{O}(1000)$. This proficiency is particularly ad-
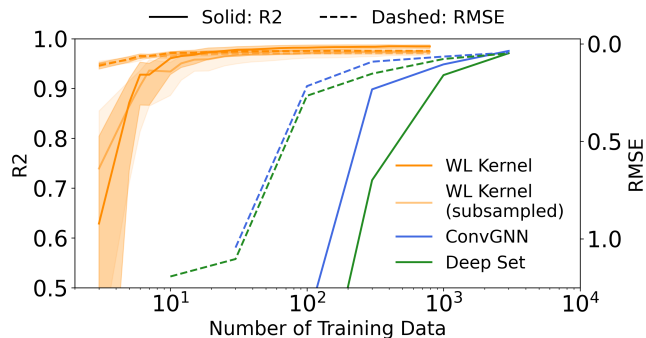
Figure 3. Performance of the WL kernel in weak chemical tagging. The plot presents the R² score and Root Mean Squared Error (RMSE) as a function of training data size, underscoring the WL kernel's effectiveness in predicting complex data structures as opposed to Deep Sets and ConvGNNs.

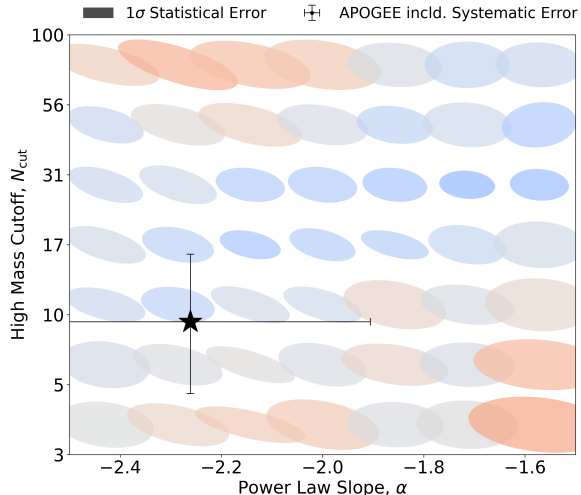*Figure 4.* Recovery of the power-law slope and high-mass cutoff via WL kernel. The ellipses illustrate the statistical errors for point clouds of 2×10^4 stars measured empirically from the mock tests. The symbol represents the limit when applying the algorithm to a well-curated, albeit incomplete, APOGEE sample of 2×10^4 stars.

vantageous when applying the WL algorithm to realistic hydrodynamical simulations, where the training limitations of ConvGNN would prove problematic.

Scalability and Interpretability: The impressive performance of the WL algorithm underlines the importance of a strong inductive bias in assessing the subtleties of star clustering in chemical space. Fig. 2 showcases how the WL approach, which implements a predetermined message passing and aggregation mechanism, as opposed to ConvGNNs, leads to robust results and enhanced interpretability. Hierarchical embedding of each node, for example, aids in identifying systematic biases such as potential biasing signals from open clusters or globular clusters.

Additionally, recognizing hierarchical signals and the inherent inductive bias enables us to make practical simplifications without substantial accuracy compromise. As demonstrated by Fig 3, even when only one in every five nodes is randomly selected in the graph during message passing, the robustness of the results is preserved. This is mainly attributable to the similarity in the node embedding in neighbouring features. Such a reduction, cutting computation by a factor of $5^2 = 25$, barely impacts the overall outcome

Prospects for Weak Chemical Tagging: Exploring the practical utility of the WL kernel, we turn our attention to Fig 4. We adjust both the high-mass cutoff N_{cut} and the power-law slope α. For this final implementation, we use a training dataset of 500. The ellipses in Fig 4 depict the empirical uncertainty derived from the test dataset, assessed via 10-fold cross-validation using the $5,000$ simulations. While some extreme conditions lead to marginal uncertainty degradation, the WL algorithm consistently produces a suitable statistical uncertainty range across a broad parameter space at the level of $0.1 - 0.2$ dex in α and $0.1 - 0.15$ dex in the logarithmic of N_{cut} with 2×10^4 stars.

For an initial trial, we apply the high-quality APOGEE

sample of 2×10^4 stars, yielding optimal values of $\alpha = -2.26^{+0.36}_{-0.32}$ and $N_{cut} = 9.4^{+7.0}_{-4.2}$, with uncertainties calculated through bootstrapping. This approach accounts for both statistical and systematic errors due to the model assumption. The derived power-law slope, α, aligns with young clusters' research (Dessauges-Zavadsky & Adamo, 2018). For the high-mass cutoff, the N_{cut} equals 9.4 for a sample size of 2×10^4, which when factored with the sampling rate, corresponds to $10^7 - 10^8 M_\odot$ (see Section 2), consistent with the globular cluster masses. The anticipated full paper will probe the global CMF constraint with a larger sample (10^7 stars) from various spectroscopic surveys, and further investigate its evolution by delving deeper into the elemental abundance space in tandem with stellar ages.

5. Broader Impact

The structure of the universe manifests in complex patterns in our observations. Decoding these patterns—astrostatistics' primary challenge—uncovers the physical parameters governing the system. Despite its power, astronomical analysis often neglects the rich information embedded in hierarchical structures, typically focusing on scalar and vector fields. Graph neural networks have disrupted this traditional field-only analysis, leveraging raw observational data in the form of point clouds of features like positions, velocities, and elemental abundances. However, they grapple with interpretability and training convergence.

This study puts forth graph kernels that can rival graph neural networks. The WL kernel's success largely stems from its strong inductive bias, effectively harnessing hierarchical information from astronomical point clouds. By address-

ing the challenge of weak chemical tagging, we introduce a first-principle approach with the potential to further Galactic Archaeology studies. Furthermore, our techniques could inspire new graph neural network applications, fostering a more statistical and fundamental approach.

References

Bensby, T., Feltzing, S., and Lundström, I. Elemental abundance trends in the Galactic thin and thick disks as traced by nearby F and G dwarf stars. *Astronomy and Astrophysics*, 410:527–551, November 2003. doi: 10.1051/0004-6361:20031213.

Buck, T., Rybizki, J., Buder, S., Obreja, A., Macciò, A. V., Pfrommer, C., Steinmetz, M., and Ness, M. The challenge of simultaneously matching the observed diversity of chemical abundance patterns in cosmological hydrodynamical simulations. *Monthly Notices of the Royal Astronomical Society*, 508(3):3365–3387, December 2021. doi: 10.1093/mnras/stab2736.

Buder, S., Sharma, S., Kos, J., Amarsi, A. M., Nordlander, T., Lind, K., Martell, S. L., Asplund, M., Bland-Hawthorn, J., Casey, A. R., De Silva, G. M., D'Orazi, V., Freeman, K. C., Hayden, M. R., Lewis, G. F., Lin, J., Schlesinger, K. J., Simpson, J. D., Stello, D., Zucker, D. B., Zwitter, T., Beeson, K. L., Buck, T., Casagrande, L., Clark, J. T., Cotar, K., Da Costa, G. S., de Grijs, R., Feuillet, D., Horner, J., Khanna, S., Kafle, P. R., Liu, F., Montet, B. T., Nandakumar, G., Nataf, D. M., Ness, M. K., Spina, L., Traven, G., Tepper-Garcia, T., Ting, Y.-S., Vogrincic, R., Wittenmyer, R. A., Zerjal, M., and the GALAH collaboration. The GALAH+ Survey: Third Data Release. *arXiv e-prints*, art. arXiv:2011.02505, November 2020.

Chen, B., Hayden, M. R., Sharma, S., Bland-Hawthorn, J., Kobayashi, C., and Karakas, A. I. Chemical Evolution with Radial Mixing Redux: Extending beyond the Solar Neighborhood. *arXiv e-prints*, art. arXiv:2204.11413, April 2022. doi: 10.48550/arXiv.2204.11413.

Dessauges-Zavadsky, M. and Adamo, A. First constraints on the stellar mass function of star-forming clumps at the peak of cosmic star formation. *Monthly Notices of the Royal Astronomical Society*, 479(1):L118–L122, September 2018. doi: 10.1093/mnrasl/sly112.

Durkan, C., Bekasov, A., Murray, I., and Papamakarios, G. Neural Spline Flows. *arXiv e-prints*, art. arXiv:1906.04032, June 2019.

Freeman, K. and Bland-Hawthorn, J. The New Galaxy: Signatures of Its Formation. *Annual Review of Astronomy and Astrophysics*, 40:487–537, January 2002. doi: 10. 1146/annurev.astro.40.060401.093840.

Fuhrmann, K. Nearby stars of the Galactic disk and halo. *Astronomy and Astrophysics*, 338:161–183, October 1998.

Gilmore, G., Randich, S., Asplund, M., Binney, J., Bonifacio, P., Drew, J., Feltzing, S., Ferguson, A., Jeffries, R., Micela, G., Negueruela, I., Prusti, T., Rix, H. W., Vallenari, A., Alfaro, E., Allende-Prieto, C., Babusiaux, C., Bensby, T., Blomme, R., Bragaglia, A., Flaccomio, E., François, P., Irwin, M., Koposov, S., Korn, A., Lanzafame, A., Pancino, E., Paunzen, E., Recio-Blanco, A., Sacco, G., Smiljanic, R., Van Eck, S., Walton, N., Aden, D., Aerts, C., Affer, L., Alcala, J. M., Altavilla, G., Alves, J., Antoja, T., Arenou, F., Argiroffi, C., Asensio Ramos, A., Bailer-Jones, C., Balaguer-Nunez, L., Bayo, A., Barbuy, B., Barisevicius, G., Barrado y Navascues, D., Battistini, C., Bellas Velidis, I., Bellazzini, M., Belokurov, V., Bergemann, M., Bertelli, G., Biazzo, K., Bienayme, O., Bland-Hawthorn, J., Boeche, C., Bonito, S., Boudreault, S., Bouvier, J., Brandao, I., Brown, A., de Bruijne, J., Burleigh, M., Caballero, J., Caffau, E., Calura, F., Capuzzo-Dolcetta, R., Caramazza, M., Carraro, G., Casagrande, L., Casewell, S., Chapman, S., Chiappini, C., Chorniy, Y., Christlieb, N., Cignoni, M., Cocozza, G., Colless, M., Collet, R., Collins, M., Correnti, M., Covino, E., Crnojevic, D., Cropper, M., Cunha, M., Damiani, F., David, M., Delgado, A., Duffau, S., Edvardsson, B., Eldridge, J., Enke, H., Eriksson, K., Evans, N. W., Eyer, L., Famaey, B., Fellhauer, M., Ferreras, I., Figueras, F., Fiorentino, G., Flynn, C., Folha, D., Franciosini, E., Frasca, A., Freeman, K., Fremat, Y., Friel, E., Gaensicke, B., Gameiro, J., Garzon, F., Geier, S., Geisler, D., Gerhard, O., Gibson, B., Gomboc, A., Gomez, A., Gonzalez-Fernandez, C., Gonzalez Hernandez, J., Gosset, E., Grebel, E., Greimel, R., Groenewegen, M., Grundahl, F., Guarcello, M., Gustafsson, B., Hadrava, P., Hatzidimitriou, D., Hambly, N., Hammersley, P., Hansen, C., Haywood, M., Heber, U., Heiter, U., Held, E., Helmi, A., Hensler, G., Herrero, A., Hill, V., Hodgkin, S., Huelamo, N., Huxor, A., Ibata, R., Jackson, R., de Jong, R., Jonker, P., Jordan, S., Jordi, C., Jorissen, A., Katz, D., Kawata, D., Keller, S., Kharchenko, N., Klement, R., Klutsch, A., Knude, J., Koch, A., Kochukhov, O., Kontizas, M., Koubsky, P., Lallement, R., de Laverny, P., van Leeuwen, F., Lemasle, B., Lewis, G., Lind, K., Lindstrom, H. P. E., Lobel, A., Lopez Santiago, J., Lucas, P., Ludwig, H., Lueftinger, T., Magrini, L., Maiz Apellaniz, J., Maldonado, J., Marconi, G., Marino, A., Martayan, C., Martinez-Valpuesta, I., Matijevic, G., McMahon, R., Messina, S., Meyer, M., Miglio, A., Mikolaitis, S., Minchev, I., Minniti, D., Moitinho, A., Momany, Y., Monaco, L., Montalto, M., Monteiro, M. J., Monier, R., Montes, D., Mora, A., Moraux, E., Morel, T., Mowlavi, N., Mucciarelli, A., Munari, U., Napiwotzki, R., Nardetto, N., Naylor, T., Naze, Y., Nelemans, G., Okamoto, S., Ortolani, S., Pace,

G., Palla, F., Palous, J., Parker, R., Penarrubia, J., Pillitteri, I., Piotto, G., Posbic, H., Prisinzano, L., Puzeras, E., Quirrenbach, A., Ragaini, S., Read, J., Read, M., Reyle, C., De Ridder, J., Robichon, N., Robin, A., Roeser, S., Romano, D., Royer, F., Ruchti, G., Ruzicka, A., Ryan, S., Ryde, N., Santos, N., Sanz Forcada, J., Sarro Baro, L. M., Sbordone, L., Schilbach, E., Schmeja, S., Schnurr, O., Schoenrich, R., Scholz, R. D., Seabroke, G., Sharma, S., De Silva, G., Smith, M., Solano, E., Sordo, R., Soubiran, C., Sousa, S., Spagna, A., Steffen, M., Steinmetz, M., Stelzer, B., Stempels, E., Tabernero, H., Tautvaisiene, G., Thevenin, F., Torra, J., Tosi, M., Tolstoy, E., Turon, C., Walker, M., Wambsganss, J., Worley, C., Venn, K., Vink, J., Wyse, R., Zaggia, S., Zeilinger, W., Zoccali, M., Zorec, J., Zucker, D., Zwitter, T., and Gaia-ESO Survey Team. The Gaia-ESO Public Spectroscopic Survey. *The Messenger*, 147:25–31, March 2012.

Griffith, E., Johnson, J. A., and Weinberg, D. H. Abundance Ratios in GALAH DR2 and Their Implications for Nucleosynthesis. *The Astrophysical Journal*, 886(2):84, December 2019. doi: 10.3847/1538-4357/ab4b5d.

Griffith, E., Weinberg, D. H., Johnson, J. A., Beaton, R., García-Hernández, D. A., Hasselquist, S., Holtzman, J., Johnson, J. W., Jönsson, H., Lane, R. R., Nataf, D. M., and Roman-Lopes, A. The Similarity of Abundance Ratio Trends and Nucleosynthetic Patterns in the Milky Way Disk and Bulge. *arXiv e-prints*, art. arXiv:2009.05063, September 2020.

Ha, T., Li, Y., Xu, S., Kounkel, M., and Li, H. Measuring Turbulence with Young Stars in the Orion Complex. *The Astrophysical Journal Letter*, 907(2):L40, February 2021. doi: 10.3847/2041-8213/abd8c9.

Jönsson, H., Holtzman, J. A., Allende Prieto, C., Cunha, K., García-Hernández, D. A., Hasselquist, S., Masseron, T., Osorio, Y., Shetrone, M., Smith, V., Stringfellow, G. S., Bizyaev, D., Edvardsson, B., Majewski, S. R., Mészáros, S., Souto, D., Zamora, O., Beaton, R. L., Bovy, J., Donor, J., Pinsonneault, M. H., Poovelil, V. J., and Sobeck, J. APOGEE Data and Spectral Analysis from SDSS Data Release 16: Seven Years of Observations Including First Results from APOGEE-South. *The Astronomical Journal*, 160(3):120, September 2020. doi: 10.3847/1538-3881/aba592.

Just, A., Piskunov, A. E., Klos, J. H., Kovaleva, D. A., and Polyachenko, E. V. Global survey of star clusters in the Milky Way. VII. Tidal parameters and mass function. *Astronomy and Astrophysics*, 672:A187, April 2023. doi: 10.1051/0004-6361/202244723.

Kingma, D. P. and Dhariwal, P. Glow: Generative Flow with Invertible 1x1 Convolutions. *arXiv e-prints*, art. arXiv:1807.03039, July 2018.

Kriege, N. M., Johansson, F. D., and Morris, C. A survey on graph kernels. *Applied Network Science*, 5(1):1–42, 2020.

Li, H., Vogelsberger, M., Marinacci, F., and Gnedin, O. Y. Disruption of giant molecular clouds and formation of bound star clusters under the influence of momentum stellar feedback. *Monthly Notices of the Royal Astronomical Society*, 487(1):364–380, July 2019. doi: 10.1093/mnras/stz1271.

Luo, A. L., Zhao, Y.-H., Zhao, G., Deng, L.-C., Liu, X.-W., Jing, Y.-P., Wang, G., Zhang, H.-T., Shi, J.-R., Cui, X.-Q., Chu, Y.-Q., Li, G.-P., Bai, Z.-R., Wu, Y., Cai, Y., Cao, S.-Y., Cao, Z.-H., Carlin, J. L., Chen, H.-Y., Chen, J.-J., Chen, K.-X., Chen, L., Chen, X.-L., Chen, X.-Y., Chen, Y., Christlieb, N., Chu, J.-R., Cui, C.-Z., Dong, Y.-Q., Du, B., Fan, D.-W., Feng, L., Fu, J.-N., Gao, P., Gong, X.-F., Gu, B.-Z., Guo, Y.-X., Han, Z.-W., He, B.-L., Hou, J.-L., Hou, Y.-H., Hou, W., Hu, H.-Z., Hu, N.-S., Hu, Z.-W., Huo, Z.-Y., Jia, L., Jiang, F.-H., Jiang, X., Jiang, Z.-B., Jin, G., Kong, X., Kong, X., Lei, Y.-J., Li, A.-H., Li, C.-H., Li, G.-W., Li, H.-N., Li, J., Li, Q., Li, S., Li, S.-S., Li, X.-N., Li, Y., Li, Y.-B., Li, Y.-P., Liang, Y., Lin, C.-C., Liu, C., Liu, G.-R., Liu, G.-Q., Liu, Z.-G., Lu, W.-Z., Luo, Y., Mao, Y.-D., Newberg, H., Ni, J.-J., Qi, Z.-X., Qi, Y.-J., Shen, S.-Y., Shi, H.-M., Song, J., Song, Y.-H., Su, D.-Q., Su, H.-J., Tang, Z.-H., Tao, Q.-S., Tian, Y., Wang, D., Wang, D.-Q., Wang, F.-F., Wang, G.-M., Wang, H., Wang, H.-C., Wang, J., Wang, J.-N., Wang, J.-L., Wang, J.-P., Wang, J.-X., Wang, L., Wang, M.-X., Wang, S.-G., Wang, S.-Q., Wang, X., Wang, Y.-N., Wang, Y., Wang, Y.-F., Wang, Y.-F., Wei, P., Wei, M.-Z., Wu, H., Wu, K.-F., Wu, X.-B., Wu, Y.-Z., Xing, X.-Z., Xu, L.-Z., Xu, X.-Q., Xu, Y., Yan, T.-S., Yang, D.-H., Yang, H.-F., Yang, H.-Q., Yang, M., Yao, Z.-Q., Yu, Y., Yuan, H., Yuan, H.-B., Yuan, H.-L., Yuan, W.-M., Zhai, C., Zhang, E.-P., Zhang, H.-W., Zhang, J.-N., Zhang, L.-P., Zhang, W., Zhang, Y., Zhang, Y.-X., Zhang, Z.-C., Zhao, M., Zhou, F., Zhou, X., Zhu, J., Zhu, Y.-T., Zou, S.-C., and Zuo, F. The first data release (DR1) of the LAMOST regular survey. *Research in Astronomy and Astrophysics*, 15(8):1095, August 2015. doi: 10.1088/1674-4527/15/8/002.

Majewski, S. R., Schiavon, R. P., Frinchaboy, P. M., Allende Prieto, C., Barkhouser, R., Bizyaev, D., Blank, B., Brunner, S., Burton, A., Carrera, R., Chojnowski, S. D., Cunha, K., Epstein, C., Fitzgerald, G., García Pérez, A. E., Hearty, F. R., Henderson, C., Holtzman, J. A., Johnson, J. A., Lam, C. R., Lawler, J. E., Maseman, P., Mészáros, S., Nelson, M., Nguyen, D. C., Nidever, D. L., Pinsonneault, M., Shetrone, M., Smee, S., Smith, V. V., Stolberg, T., Skrutskie, M. F., Walker, E., Wilson, J. C., Zasowski, G., Anders, F., Basu, S., Beland, S., Blanton, M. R., Bovy, J., Brownstein, J. R., Carlberg, J.,

Chaplin, W., Chiappini, C., Eisenstein, D. J., Elsworth, Y., Feuillet, D., Fleming, S. W., Galbraith-Frew, J., García, R. A., García-Hernández, D. A., Gillespie, B. A., Girardi, L., Gunn, J. E., Hasselquist, S., Hayden, M. R., Hekker, S., Ivans, I., Kinemuchi, K., Klaene, M., Mahadevan, S., Mathur, S., Mosser, B., Muna, D., Munn, J. A., Nichol, R. C., O'Connell, R. W., Parejko, J. K., Robin, A. C., Rocha-Pinto, H., Schultheis, M., Serenelli, A. M., Shane, N., Silva Aguirre, V., Sobeck, J. S., Thompson, B., Troup, N. W., Weinberg, D. H., and Zamora, O. The Apache Point Observatory Galactic Evolution Experiment (APOGEE). *The Astronomical Journal*, 154:94, September 2017. doi: 10.3847/1538-3881/aa784d.

Mok, A., Chandar, R., and Fall, S. M. Constraints on Upper Cutoffs in the Mass Functions of Young Star Clusters. *The Astrophysical Journal*, 872(1):93, February 2019. doi: 10.3847/1538-4357/aaf6ea.

Morris, C., Kersting, K., and Mutzel, P. Glocalized weisfeiler-lehman graph kernels: Global-local feature maps of graphs. In *2017 IEEE International Conference on Data Mining (ICDM)*, pp. 327–336. IEEE, 2017.

Ness, M., Rix, H. W., Hogg, D. W., Casey, A. R., Holtzman, J., Fouesneau, M., Zasowski, G., Geisler, D., Shetrone, M., Minniti, D., Frinchaboy, P. M., and Roman-Lopes, A. Galactic Doppelgängers: The Chemical Similarity Among Field Stars and Among Stars with a Common Birth Origin. *The Astrophysical Journal*, 853(2):198, February 2018. doi: 10.3847/1538-4357/aa9d8e.

Price-Jones, N. and Bovy, J. The dimensionality of stellar chemical space using spectra from the Apache Point Observatory Galactic Evolution Experiment. *Monthly Notices of the Royal Astronomical Society*, 475(1):1410–1425, March 2018. doi: 10.1093/mnras/stx3198.

Schulz, T. H., Horváth, T., Welke, P., and Wrobel, S. A generalized weisfeiler-lehman graph kernel. *Machine Learning*, 111(7):2601–2629, 2022.

Shervashidze, N., Schweitzer, P., van Leeuwen, E. J., Mehlhorn, K., and Borgwardt, K. M. Weisfeiler-lehman graph kernels. *J. Mach. Learn. Res.*, 12:2539–2561, 2011.

Smith, J. D., Dale, J. E., Jaffa, S. E., and Krause, M. G. H. Star cluster formation in clouds with externally driven turbulence. *Monthly Notices of the Royal Astronomical Society*, 516(3):4212–4219, November 2022. doi: 10.1093/mnras/stac2295.

Spina, L., Magrini, L., Sacco, G. G., Casali, G., Vallenari, A., Tautvaišienė, G., Jiménez-Esteban, F., Gilmore, G., Randich, S., Feltzing, S., Jeffries, R. D., Bensby, T., Bragaglia, A., Smiljanic, R., Carraro, G., Morbidelli,

L., and Zaggia, S. The Gaia-ESO Survey: Chemical tagging in the thin disk. Open clusters blindly recovered in the elemental abundance space. *Astronomy and Astrophysics*, 668:A16, December 2022. doi: 10.1051/0004-6361/202243316.

Ting, Y.-S., Conroy, C., and Goodman, A. Prospects for Chemically Tagging Stars in the Galaxy. *The Astrophysical Journal*, 807(1):104, July 2015. doi: 10.1088/0004-637X/807/1/104.

Ting, Y.-S., Conroy, C., and Rix, H.-W. APOGEE Chemical Tagging Constraint on the Maximum Star Cluster Mass in the Alpha-enhanced Galactic Disk. *The Astrophysical Journal*, 816(1):10, January 2016. doi: 10.3847/0004-637X/816/1/10.

Vincenzo, F., Weinberg, D. H., Miglio, A., Lane, R. R., and Roman-Lopes, A. The distribution of [α/Fe] in the Milky Way disc. *arXiv e-prints*, art. arXiv:2101.04488, January 2021.

Weinberg, D. H., Holtzman, J. A., Hasselquist, S., Bird, J. C., Johnson, J. A., Shetrone, M., Sobeck, J., Allende Prieto, C., Bizyaev, D., Carrera, R., Cohen, R. E., Cunha, K., Ebelke, G., Fernandez-Trincado, J. G., García-Hernández, D. A., Hayes, C. R., Jönsson, H., Lane, R. R., Majewski, S. R., Malanushenko, V., Mészáros, S., Nidever, D. L., Nitschelm, C., Pan, K., Rix, H.-W., Rybizki, J., Schiavon, R. P., Schneider, D. P., Wilson, J. C., and Zamora, O. Chemical Cartography with APOGEE: Multi-element Abundance Ratios. *The Astrophysical Journal*, 874(1):102, March 2019. doi: 10.3847/1538-4357/ab07c7.